Available online at www.sciencedirect.com
ScienceDirect
Journal of Power Sources 158 (2006) 1394–1400
JOURNAL OF POWER SOURCES
www.elsevier.com/locate/jpowsour

First-principles calculations on the Jahn–Teller distortion in layered $LiMnO_2$

Zu-Fei Huang, Xing Meng, Chun-Zhong Wang, Yuan Sun, Gang Chen *

Department of Materials Science, College of Materials Science and Engineering, Jilin University, Changchun 130012, PR China

Received 1 August 2005; received in revised form 3 October 2005; accepted 16 October 2005
Available online 28 November 2005

Abstract

First-principles calculations within the spin-polarized generalized gradient approximation framework are performed on rhombohedral and its Jahn–Teller distorted monoclinic $LiMnO_2$ with different spin configurations. It is found that the Jahn–Teller (JT) effect is driven by high-spin Mn^{3+} ion and it should disappear in low-spin state. With JT distortion, the initially degenerate e_g states is split by a gap of 687 meV, which responds for the semiconduction of monoclinic $LiMnO_2$. Based on the analyses of the changes induced by JT distortion in the crystal, electronic structures and chemical bondings, approaches to suppress the JT effect and synthesize rhombohedral $LiMnO_2$ are suggested. At last, the JT effect is decomposed into an electronic and an elastic term.

Keywords: Layered $LiMnO_2$; Ab initio investigation; Jahn–Teller effect; Electronic structures; Chemical bondings

1. Introduction

Because monoclinic $LiMnO_2$ (space group $C2/m$, hereafter denoted as m-$LiMnO_2$) has a high theoretical capacity (285 mAh g^{-1}) and Mn is abundant, inexpensive and environmentally benign, intense expectation has been put on this material to replace $LiCoO_2$, the current standard cathode material in commercial Li-ion rechargeable batteries since it was first obtained by ion exchange from α-$NaMnO_2$ in 1996 [1,2]. This compound has a layered structure where Li^+, Mn^{3+} and O^{2-} locate in their own triangular planes, respectively, and these planes stack with a sequence as Li–O–Mn–O–Li. The O^{2-} sublattice is fcc and simply provides a framework with Li^+ and Mn^{3+} filling all the interstices of its edge-shared octahedrons. Such a layered structure is similar to that of $LiCoO_2$ and has superior Li de-intercalation cycling properties than that of its stable form, orthorhombic $LiMnO_2$ ($Pmnm$, o-$LiMnO_2$) [1–5]. Experimentally, a large initial capacity of more than 270 mAh g^{-1} has been measured [1].

However, m-$LiMnO_2$ suffers from severe capacity fading, which is surely ascribable to the irreversible transition to a spinel-like structure and is the primary obstacle to its applications in practice [3–5]. Such a structural instability is caused by the wide and discontinuous variation in the magnitude of the Jahn–Teller (JT) distortion because the Mn ions are cycled between JT active high-spin Mn^{3+} and inactive Mn^{4+} states during the electrochemical charge–discharge process [5,7]. Therefore, JT effect plays an important role in the applications of this electrochemical material and deserves detailed investigation. JT effect operates due to partial-filled electronic subshell, distorting the crystal structure to eliminate the degeneracy until the increase in elastic energy halts the distortion [5–7].

Because m-$LiMnO_2$ is the JT distorted form of rhombohedral $LiMnO_2$ ($R\bar{3}m$, r-$LiMnO_2$), we carry out first-principles calculations on the crystal and electronic structures of both m- and r-$LiMnO_2$ with different spin configurations to investigate the JT effect in m-$LiMnO_2$. Previous reports have concluded that generalized gradient approximation (GGA) achieves greater accuracy for Mn-oxides compared with local density approximation (LDA) [8]. In addition, Mn^{3+} ions in both the structures are magnetic. Therefore, spin-polarized GGA-PW91 (GGS-PW91) [9] is employed for the exchange-correlation potential.

* Corresponding author. Tel.: +86 431 5168446; fax: +86 431 5168446.
E-mail address: gchen@jlu.edu.cn (G. Chen).

0378-7753/$ – see front matter © 2005 Elsevier B.V. All rights reserved.
doi:10.1016/j.jpowsour.2005.10.044

2. Computational details

All the calculations are performed with the CASTEP software [9]. The initial crystal model of *m*-$LiMnO_2$ is built using the experimental lattice parameters and ionic positions [1] but neglecting the ~10% Li/Mn site disorder, while hypothetical *r*-$LiMnO_2$ has isostructure to that of $LiCoO_2$ [10] but substituting all Co with Mn. Primitive cells containing one formula unit are investigated. In an octahedral complex, the five d orbitals of a transition metal ion will be split into a set of lower three-fold degenerate t_{2g} states and upper two-fold degenerate e_g states according to ligand field theory [6,7]. Therefore, Mn^{3+} (d^4) ion can have three spin configurations as high-spin ($t_{2g}^3e_g^1$), low-spin ($t_{2g}^4e_g^0$ and occupying all three t_{2g} levels) or non-spin ($t_{2g}^4e_g^0$ and occupying two of the three t_{2g} levels) states, which is stimulated by fixing the spin, unpaired electrons in the cell, as 4, 2 or 0 under neutralizing background, respectively. Ultrasoft pseudo-potentials in the reciprocal space are employed with a plane-wave energy cutoff of 400 eV. Requested *k*-point spacing is set to 0.05 $Å^{-1}$, which corresponds to 72 *k*-points for *m*-$LiMnO_2$ and 60 *k*-points for *r*-$LiMnO_2$ in the irreducible Brillouin zone generated by the Monkhorst–Pack scheme. Geometry optimization is first performed to fully relax the structures until self-consistent field (SCF) convergence per atom, tolerances for total energy, root-mean-square (RMS) displacement of atoms, RMS force on atoms and RMS stress tensor are less than 2×10^{-6} eV, 2×10^{-5} eV, 0.001 Å, 0.05 eV/Å and 0.1 GPa, respectively. Then, the relaxed structures were used to calculate the total energies and the electronic structures with the same energy cutoff and *k*-points as those the geometrical optimizations used. Because *m*-$LiMnO_2$ shows a spin-glass ground state where short-range anti-ferromagnetic (AF) and ferromagnetic (FM) interactions are coexistent randomly [3], for the restriction of invoked periodic-boundary conditions during the calculations, only FM ordering was considered with disregarding the AF cases.

3. Results and discussion

The calculated relative total energies (ΔE), magnetic moments at each Mn site (*M*) and lattice parameters (*a*, *b*, *c* and β) of the relaxed crystal structures together with the experimental and theoretical data are listed in Table 1. As proven by *M* obviously, the high-spin, low-spin and non-spin states have been reproduced successfully (the reduction of *M* from the nominal Hund's rule value for high-spin state, i.e. *M* are not equal to but less than 4.0, will be discussed below in the section of partial density of states). From the viewpoint of energy, non-spin state is instable distinctly to low-spin and high-spin states for both symmetries, so this spin configuration will not be considered hereafter. For high-spin state, because of the energy benefit as large as 175 meV, the JT effect will usually take place during the progress of synthesis where the experimental condition can supply the additional energy to overcome the energy barrier to the transition, and thereby *m*-$LiMnO_2$ but not *r*-$LiMnO_2$ is obtained. As to low-spin state, situation is discussible because the energy benefit from JT distortion is too small (only 8 meV). Such small value may locate in the calculation error and more importantly, according to the argument of Ceder et al., a small enough (less than 30 meV) formation enthalpy allows for entropy-driven mixing [11]. In the same way, low-spin state of *r*-$LiMnO_2$ can be stabilized to high-spin state with an energy barrier of only 11 meV. Experimentally, high-spin state for *m*-$LiMnO_2$ and low-spin state for *r*-$LiMnO_2$ also reproduce compatible lattice parameters with measured data (see Table 1) [1,12]. Because pure *r*-$LiMnO_2$ is still hypothetical, the Cr-doped experimental data are used here [12]. Theoretically, other groups have found a low-spin Mn^{3+} ion in *r*-$LiMnO_2$, too [5,7,8]. Therefore, it is concluded that the JT distortion in layered $LiMnO_2$ is driven by the high-spin Mn^{3+} ion, resulting in *m*-$LiMnO_2$. While for low-spin state, JT distortion is absent and *r*-$LiMnO_2$ should be obtained.

Table 1 also gives the nearest Mn–Mn distances, which are equal to the lattice parameter *b*, cell volumes (*V*) per formula

Table 1
Calculated magnetic moments at each Mn sites (*M*), relative total energies (ΔE) and cell volumes (*V*) per formula unit, optimized lattice parameters (*a*, *b*, *c* and β), Mn—O bond lengths (L_{Mn-O}) and Jahn–Teller distortion degree (JT) of *r*- and *m*-$LiMnO_2$ under different spin configurations (S_{fix}) together with experimental and theoretical data

S_{fix}	Cell	M_{Mn} (μ_B)	ΔE (meV)	*a* (Å)	*b* (Å)	*c* (Å)	β (°)	*V* (Å^3)	L_{Mn-O} (Å)	JT (%)
4	*r*-$LiMnO_2$	3.80	0	$a=b=3.0045$		14.7392	90	38.4085	2.0665×6	0
	m-$LiMnO_2$	3.72	−175	5.5497	2.8623	5.4365	116.575	38.6167	2.3707×2, 1.9679×4	20.02
2	*r*-$LiMnO_2$	2.00	11	$a=b=2.8664$		14.6002	90	34.6296	2.0021×6	0
	m-$LiMnO_2$	2.00	3	4.9818	2.8628	5.1237	109.315	34.4801	2.0023×2, 2.0014×4	0.04
0	*r*-$LiMnO_2$	0.00	630	$a=b=2.8409$		14.4659	90	33.7034	1.9916×6	0
	m-$LiMnO_2$	0.00	659	5.0030	2.8675	5.0760	109.684	34.2826	2.0007×2, 1.9896×4	0.56
Experimental	*r*-$LiMnO_2$ [12]	–	–	$a=b=2.8799$		14.3799	90	34.4287	1.9718×6	0
	m-$LiMnO_2$ [1]	–	–	5.4387	2.8086	5.3878	116.006	36.9837	2.3079×2, 1.9211×4	18.87
Theoretical	*r*-$LiMnO_2$ [8]	~2.0	–	$a=b=2.82$		14.27	90	32.76	1.97×6	0
	m-$LiMnO_2$ [8]	~4.0	–	5.54	2.82	5.44	116	38.19	2.34×2, 1.92×4	20.39

unit and Mn–O bond lengths ($L_{Mn–O}$). It is noted that with the JT distortion, $L_{Mn–O}$ in the regular MnO_6 octahedron have split into two sets: two are elongated but the other four shortened. Defining JT distortion degree as the difference between the longest and shortest Mn–O distances divided by the average Mn–O distance [3,8], large JT distortion (20.02%) are detected for high-spin state, while for low-spin state, it is too small (only 0.04%) to be detected experimentally. Furthermore, the JT transition temperature (T_t) and the JT distortion degree c/a (here c and a refer to the inner parameters of MnO_6 octahedron but not the lattice parameters) have a moderate correlation to the electronic structure of the MnO_6 octahedron because of the thermal excitation of electrons over the energy gap Δ between the d_{z^2} and $d_{x^2-y^2}$ orbital of e_g states in the JT distorted, tetragonal symmetry [13],

$$\Delta \sim k_B T_t \propto (c/a - 1) \tag{1}$$

For $c/a = 1.15$ and $T_t = 1400$ K [13], we can extrapolate $T_t = 1910$ K for high-spin state with c/a being 1.20. Obviously, m-$LiMnO_2$ is molten at this temperature, which implies that in high-spin state the JT distortion always exists in the crystalline structure and non-JT distorted r-$LiMnO_2$ cannot be synthesized, agreeing well with the experiments [1–7]. For low-spin state, $T_t = 4$ K, which means that JT distortion will disappear at the temperature higher than 4 K and the material will adopt the rhombohedral structure. That is to say, in order to obtain r-$LiMnO_2$, one should manage to keep the material in the low-spin state, reinforcing the conclusion above.

In order to compare the lattice parameters in the same scale, monoclinic $C2/m$ symmetry can be indexed by the equivalent lattice parameters a_m and c_m like as in the $R\bar{3}m$ structure: a_m is calculated from the area of the triangular net (S) and c_m from the interlayer distance (D) based on the relation between these two structures [4]. In both the structures, the Li^+, Mn^{3+} and O^{2-} ions form respective triangular layers, and these layers stack with a sequence as Mn–O–Li–O–Mn. Differently, for $R\bar{3}m$ structure, the triangular net of the layer is equilateral with the side indexed as the a parameter, therefore, $S = 1/2 \times a \times \sqrt{3}a/2$. Because its unit cell contains three periods of the sequence which is stacked vertically and the total interlayer distance is indexed by the c parameter, $D = 1/3 \times c$. While for $C2/m$ structure, JT distortion has deformed the equilateral triangular net of the layers to be isosceles triangle and the unit cell contains only one period of the sequence which is not stacked vertically any longer, making $S = 1/2 \times b \times a/2$ and $D = c \times \sin\beta$. Therefore,

$$a_m = \left(\frac{a \times b}{\sqrt{3}}\right)^{1/2}, \qquad c_m = 3c \times \sin\beta \tag{2}$$

Values of $a_m = 2.9849$ Å, $c_m = 14.5864$ Å and $a_m = 2.8695$ Å, $c_m = 14.5059$ Å are obtained for high-spin and low-spin states of m-$LiMnO_2$, respectively, where a_m is larger and c_m is smaller than those for r-$LiMnO_2$ with the same spin configuration (see Table 1). It is interesting to note that the relaxation is not achieved by simply dispersing all the ions in the layers but by making two of the six coordinates around one ions closer along the b axis and the other four much farther, just like the change in the MnO_6 octahedron as revealed by the nearest Mn–Mn distances b (see Table 1). At the same time, V increases in high-spin state but decreases in low-spin states. These changes with JT distortion imply that JT distortion has compressed the structure perpendicularly to the triangular layers but relaxed the structure in the layers, and the compression dominates in low-spin state while the relaxation dominates in high-spin state. Therefore, in order to suppress the JT effect, endeavors should be introduced to weaken the interaction between the layers but strengthen the interaction in the layers. Such a finding can answer for the experimental fact that Co-doped r-$LiMnO_2$ can be synthesized and it tends to form non-stoichiometric materials [5], because the absence of Li can enhance the electrostatic repulsion between the nearest O–O layers.

As described in the introduction, Mishra and Ceder [8] have performed similar theoretical calculations on the material with special emphasis on the ground states. Their results for FM solution with GGS method [8] are quoted in the last two rows of Table 1. They reported that the low-spin and high-spin states are the ground state of r- and m-$LiMnO_2$, respectively, consistent with our conclusion. Nevertheless, it is noticeable that under the same spin states our values for the lattice parameters, V and $L_{Mn–O}$ are all larger than theirs, which is more distinct for r-$LiMnO_2$. We ascribe it to the full relaxation of our structures because of the severe computational conditions used during the geometry optimization. Obviously, full relaxation is very important and necessary for hypothetical r-$LiMnO_2$.

Figs. 1 and 2 show the band structures around the Fermi level (E_F) for high-spin and low-spin states before and after JT distortion, respectively. E_F is set as 0 eV, and the spin-up/down sub-bands are plotted separately as denoted by "up"/"down" in the figures. Fig. 3 is the corresponding density of states (DOS). According to the schematic picture for the band structures of octahedrally coordinated solids [14], the top five bands are assigned to Mn-3d bands and the bottom six are O-2p bands, because they mainly consist of Mn-3d and O-2p states, respectively. An unoccupied bands located around 10 eV is mainly made up of Li-2s and Mn-4s, 4p states, and the valence bands at about −18 and −45 eV are O-2s and Li-1s states, respectively (not shown in the figures). Such assignments are proven directly by the partial DOS as shown in Fig. 3. Because of the ligand field effect, the Mn-3d bands have split into upper two e_g bands and lower three t_{2g} bands by a direct gap (Δ_O).

For high-spin state, the ground state of m-$LiMnO_2$ as proven above, one can note that the most distinct changes in the bands structures with JT distortion are that the two e_g bands have been split by a gap of 687 meV which responds for the semiconduction of this material, and Δ_O has decreased. Such a splitting eliminates the degeneracy in half-filled e_g bands and lowers the energy of the electrons, thereby the system's energy. The later cannot be read out directly from the bands because the E_F is fixed at 0 eV. For comparison these bands on an "absolute" energy scale, we can align the Li-1s (or O-2s) states based on the assumption

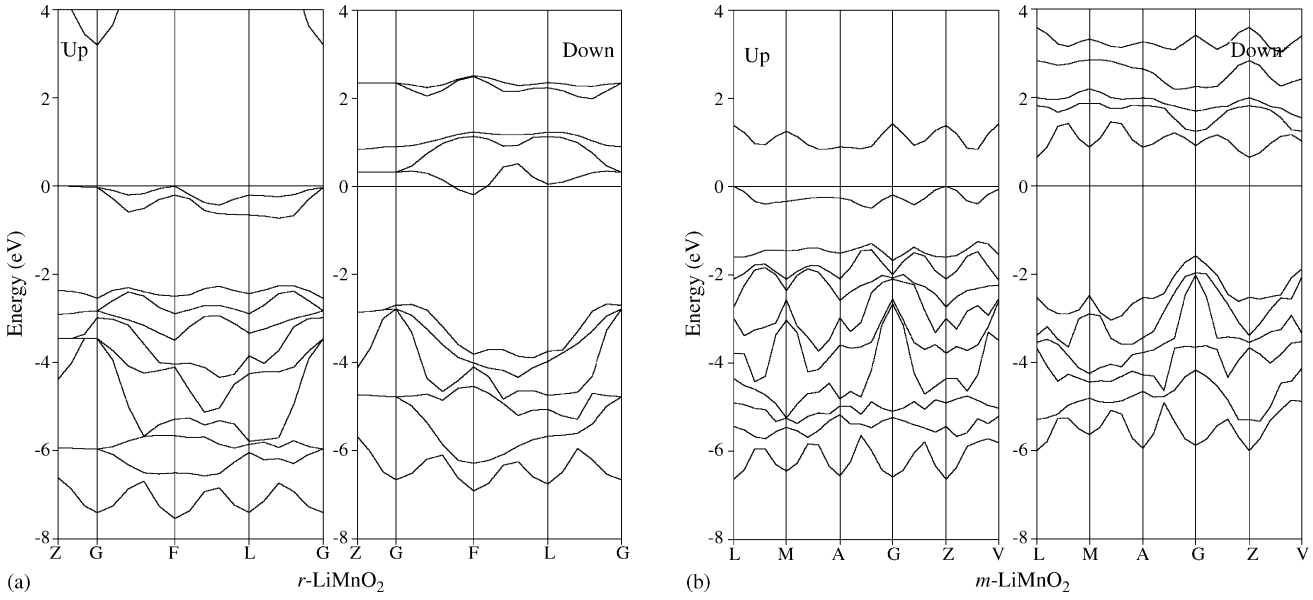

Fig. 1. Band structures for high-spin state before (a) and after (b) JT distortion.

that these states are core states and should not be affected by the different environments and therefore can be used as a reference [15]. In order to operate this alignment, it is found that the E_F for *m*-$LiMnO_2$ should shift down by 1.041 eV (see Fig. 3). That is to say, e_g bands have shifted down about 1.041 eV with JT distortion. However, the level of t_{2g} bands remains almost fixed because of its non-bonding character. Therefore, it is inevitable that Δ_O decreases dramatically. The decrease in Δ_O also consists to the stretching of the MnO_6 octahedron caused by JT distortion, because Δ_O characterizes the strength of the ligand field and compressing the Mn–O bond length would lead to its increase [14,16]. When the compressing is considerable enough to split these two bands to the point where the spin-up e_g levels rise above the lowest spin-down t_{2g} level, low-spin state would be obtained from the high-spin state [16].

Actually, it is just the splitting of e_g bands that reflects the JT effect on the electronic structures and characterizes the JT distortion degree [6,13,17]. Because of the negligible JT distortion for low-spin state as revealed above, it is not strange that the change in its two e_g bands is small and they are still degenerate (see Figs. 2 and 3). Here, it is necessary to point out that JT effect splits the e_g bands with the same spin orientations in both

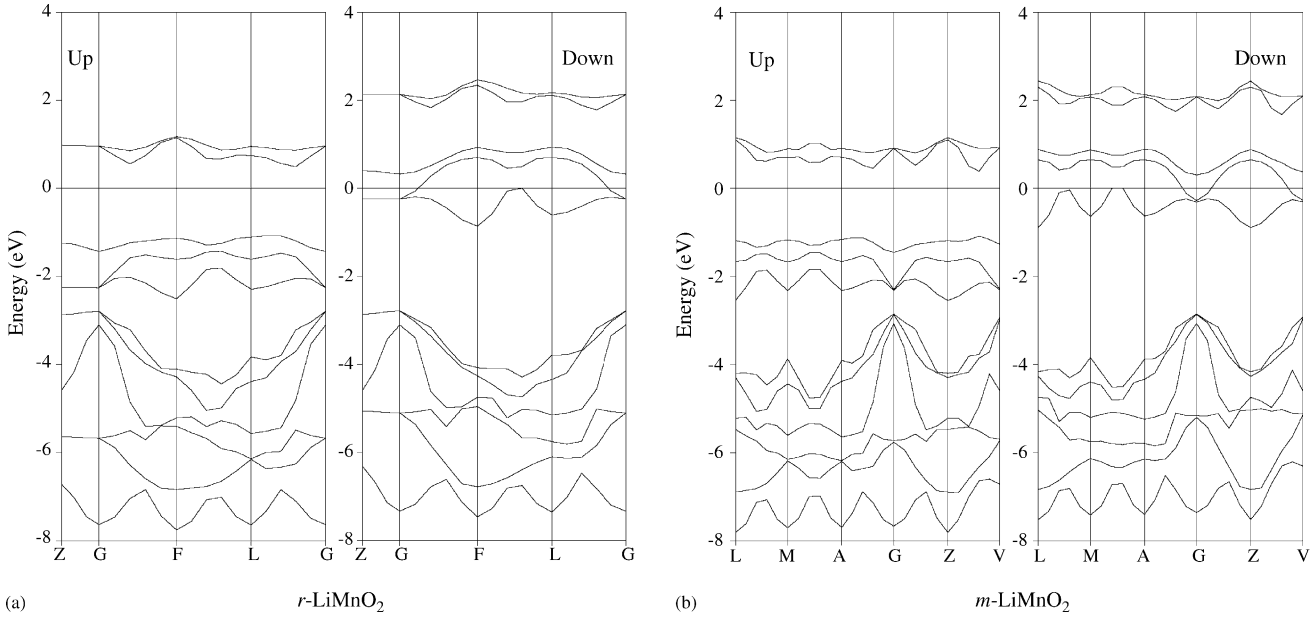

Fig. 2. Band structures for low-spin state before (a) and after (b) JT distortion.

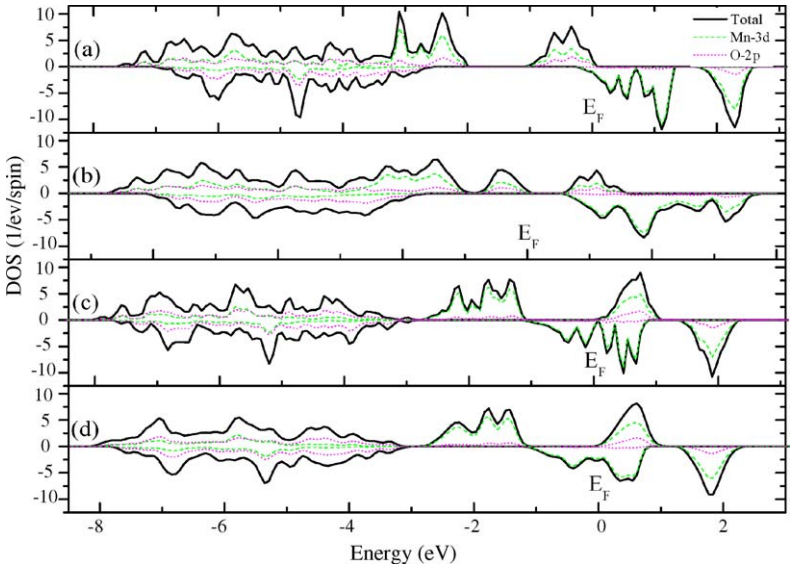

Fig. 3. DOS for high-spin state before (a) and after (b) JT distortion as well as for low-spin state before (c) and after (d) JT distortion. Spin-up/down states are plotted along the positive/negative ordinate. In this energy range, the contributions of Li-s, Mn-s, Mn-p and O-s are small and are not shown. The energy axes have been aligned as described in the text.

spin-up and spin-down sub-bands, while the splitting between these two spin species is caused by intra-ionic exchange [16,18] which has been treated wrongly as JT effect splitting in Ref. [7]. As expected, the exchange splitting Δ_{exch} is similar before and after JT distortion because of the similar M (see Table 1). Taking Δ_{exch} as the energy difference between the midpoints of the spin-up and spin-down t_{2g} bands [18], an order of 3.4 and 1.8 eV can be calculated for high-spin and low-spin states, respectively.

In Fig. 3, significant mixing of spin-up Mn-3d states in O-2p bands as well as O-2p states in e_g bands can be noted in all compounds, which reveals strong hybridization between Mn-3d and O-2p states and the bonding, anti-bonding and non-bonding characters of O-2p, e_g and t_{2g} bands, respectively. This hybridization leads to three consequences: the first is the exchange splitting of O-2p bands because of the exchange splitting of e_g states; the second is the reduction of M from the nominal Hund's rule value for high-spin state (see Table 1) with the residual magnetic moment on the O ions, because the partially filled e_g states are spin polarization; the third is the partial ionization of O ions because the e_g states are not fully occupied. Similar results are reported in Singh's work where M is only 3.45 μ_B and Δ_{exch} of O-2p bands is about 0.6 eV [19]. At the same time, Li ion is fully ionized as revealed by the absence of Li-2s states near E_F. In order to keep the electric neutrality, therefore, Mn ion is partially ionized, too. That is to say, the number of 3d electrons for Mn ion is larger than 4, which responds to the deviation from the normal ionic scenario in the band structures, where more than four t_{2g} bands lie below E_F for low-spin state and the E_F for high-spin m-$LiMnO_2$ locates above the spin-up e_g bands rather than in the middle of them.

The large degree of hybridization also indicates strong covalent interaction between Mn and O ions. For more detailed and deeply discussion, Mulliken population analysis is performed and the results are listed in Table 2. The strength of the covalent/ionic interaction between two ions is characterized by a positive/negative value of the bond overlap populations (OP). The large deviation from the formal charges of Mn and O ions confirms that the Mn–O bonds are strongly covalent, which is reinforced by the large positive values of corresponding OP. Comparably, it is clear the Li ions has been absolutely ionized and the Li–O bonds are ionic property. Similar pictures occur in other lithium transition metal oxides and it is found vital to the materials' electrochemical performance and optimization [11,14,19–21]. For high-spin state, it is found that the JT distortion has increased slightly the ionicities of Li from +1.03 to +1.04 but decreased the ionicities of Mn and O ions from +0.61, −0.82 to +0.58, −0.81, respectively. As revealed by the increase in OP values and decrease in the bond lengths, the ionic interaction in Li–O bonds and the covalent interaction in Mn–O bonds are both enhanced, which implies that the Li ion also participates in the JT distortion [22] and the average intercalation voltage of m-$LiMnO_2$ will increase [23]. Additionally, it reveals that in high-spin state m-$LiMnO_2$, the JT distorted form, is more stable over r-$LiMnO_2$, which agrees well with the experiments. While for low-spin state, the changes caused by JT distortion are almost negligible (see Table 2), which consists with the little structure differences and the comparable total energies between these two symmetries and thereby supports the above conclusion that it's possible to synthesize r-$LiMnO_2$ by compressing the Mn–O bond to keep the Mn^{3+} ion in low-spin state.

Based on the aligned total DOS (Fig. 3), we can calculate the change with JT distortion in the total electronic energy per formula unit (ΔE_{elec}) by evaluating Eq. (3) [6]. The limits of integration are from the lowest Li-1s state to the E_F. Values of −3.876 and −0.640 eV are calculated for high-spin and

Table 2
The net charges of Li, Mn and O ions, bond overlap populations (OP) of Li—O, Mn—O bonds and the corresponding bond lengths (L) before (r-$LiMnO_2$) and after (m-$LiMnO_2$) JT distortion for high-spin and low-spin states

S_{fix}	Cell	Li	Mn	O	OP_{Li-O}	L_{Li-O} (Å)	OP_{Mn-O}	L_{Mn-O} (Å)
4	r-$LiMnO_2$	+1.03	+0.61	−0.82	−0.02	2.1879	+0.88	2.0665
	m-$LiMnO_2$	+1.04	+0.58	−0.81	−0.04	2.1008	+0.90	1.9679
2	r-$LiMnO_2$	+1.05	+0.42	−0.73	−0.06	2.1086	+0.98	2.0021
	m-$LiMnO_2$	+1.06	+0.41	−0.73	−0.06	2.0929	+0.98	2.0014

low-spin states, respectively. In the simplest description for the JT distortion, the JT stabilization energy consists of two parts: an electronic term that is linear in the distortion (δ) and an elastic term that varies quadratic with δ, which can be written as Eq. (4) [6,22], where λ is the electron–phonon coupling parameter and k is an elastic constant. Roughly, E_{JT} equals to the decrease in the total energies ΔE. Therefore, the increase in the elastic energies, i.e. the second term in Eq. (4) can be calculated by the difference of ΔE and ΔE_{elec}. With the definition of δ as the difference between the longest and shortest Mn–O distances in the elongated octahedron, we can obtain $\lambda = -9.623\,eV/Å$, $k = 45.622\,eV/Å^2$ and $\lambda = -711.111\,eV/Å$, $k = 1.560 \times 10^6\,eV/Å^2$ for high-spin m-$LiMnO_2$ and low-spin m-$LiMnO_2$. Obviously, the later k value is too large to be reasonable, which reinforces the conclusion again that in low-spin state, the JT distortion should not take place and the material should have the $R\bar{3}m$ symmetry. In another words, r-$LiMnO_2$ should be stabilized over m-$LiMnO_2$ in low-spin state.

$$E_{elec} = \int \varepsilon \times N(\varepsilon)\,d\varepsilon \tag{3}$$

$$E_{JT} = \lambda\delta + \frac{1}{2}k\delta^2 \tag{4}$$

4. Conclusions

First-principles calculations in the GGS have been employed to investigate the JT effect in layered $LiMnO_2$, r-$LiMnO_2$ and its JT distorted form m-$LiMnO_2$, with different spin configurations. It is found that non-spin state is instable for both the symmetries. In low-spin state, JT effect should be absent and the layered structure should be stabilized in r-$LiMnO_2$, which may be realized by managing to compress the Mn–O bond. Only in high-spin state, JT effect is active with an energy benefit of 175 meV and the layered structure adopts the form of m-$LiMnO_2$, which agrees well with the experiment. Through JT distortion, regular MnO_6 octahedron has been elongated with a degree as large as 20.02%, and thereby it is predicted that the JT distortion will vanish at 1910 K. Simultaneously, JT distortion has compressed the structure perpendicularly to the triangular layers but relaxed in the layers as well as a slight expansion of 0.54% in the volume, which directs useful ways to suppress the JT distortion. JT distortion also leads to distinct changes in the electronic structures, where the initially degenerate e_g bands have been open by a direct gap of 687 meV and the ligand field splitting has decreased remarkably. In chemical bondings, JT effect has increased the ionicities of Li ion but decreased that of Mn and O ions. The ionic interaction in Li–O bonds as well as the covalent interaction in Mn–O bonds has been enhanced, and the participation of Li ion in the JT effect is detected. At last, the JT stabilization energy of m-$LiMnO_2$ has decomposed into an electronic term of 3.876 eV and an elastic term of −3.701 eV, where the corresponding electron–phonon coupling parameter and elastic constant has been calculated ab initio as $-9.623\,eV/Å$ and $45.622\,eV/Å^2$, respectively.

Acknowledgements

This work was sponsored by both the Chinese Natural Science Foundation, under Grant No. 50272023, the Special Funds for Major State Basic Research Project of China under Grant No. 2002CB211802 and a component part of Key Project 10411 from the Ministry of Education, China.

References

[1] A.R. Armstrong, P.G. Bruce, Nature (London) 381 (1996) 499.
[2] F. Capitaine, P. Gravereau, C. Delmas, Solid State Ionics 89 (1996) 197.
[3] G. Ceder, S.K. Mishra, Electrochem. Solid-State Lett. 2 (1999) 550.
[4] Y. Koyama, Y. Makimura, T. Ohzuku, H. Adachi, T. Uhuru, J. Electrochem. Soc. 151 (2004) A1499.
[5] R. Prasad, R. Benedek, A.J. Kropf, C.S. Johnson, A.D. Robertson, P.G. Bruce, M.M. Thackeray, Phys. Rev. B 68 (2003) 012101.
[6] C.A. Marianetti, D. Morgan, G. Ceder, Phys. Rev. B 63 (2001) 224304.
[7] T. Amriou, B. Khelifa, H. Aourag, S.M. Aouadi, C. Mathieu, Mater. Chem. Phys. 92 (2005) 499.
[8] S.K. Mishra, G. Ceder, Phys. Rev. B 59 (1999) 6120.
[9] (a) Acers Inc., CASTEP Users Guide, Accelrys Inc., San Diego, 2001;
(b) V. Mailman, B. Winkler, J.A. White, C.J. Pickard, M.C. Payne, E.V. Akhmatskaya, R.H. Nobes, Int. J. Quant. Chem. 77 (2000) 895;
(c) J.P. Perdew, Y. Wang, Phys. Rev. B 46 (1992) 6671;
(d) J.A. White, D.M. Bird, Phys. Rev. B 50 (1994) 4954.
[10] X.G. Xu, C. Li, J.X. Li, U. Kolb, F. Wu, G. Chen, J. Phys. Chem. B 107 (2003) 11648.
[11] G. Ceder, Y.-M. Chiang, D.R. Sadoway, M.K. Aydinol, Y.-I. Jang, B. Huang, Nature 392 (1998) 694.
[12] S.T. Myung, S. Komaba, N. Hirosaki, N. Kumagai, K. Arai, R. Kodama, I. Nakai, J. Electrochem. Soc. 150 (2003) A1560.
[13] A. Yamada, M. Tanaka, K. Tanaka, K. Sekai, J. Power Sources 81–82 (1999) 73.
[14] M.K. Aydinol, A.F. Kohan, G. Ceder, K. Cho, J. Joannopoulos, Phys. Rev. B 56 (1997) 1354.
[15] K. Ramesha, R. Seshadri, C. Ederer, T. He, M.A. Subramanian, Phys. Rev. B 70 (2004) 214409.
[16] A. Van der Ven, C. Marianetti, D. Morgan, G. Ceder, Solid State Ionics 135 (2000) 21.

[17] Y.J. Wei, X.G. Xu, C.Z. Wang, C. Li, G. Chen, Appl. Phys. Lett. 83 (2003) 1791.
[18] M. Lauer, R. Valenti, H.C. Kandpal, R. Seshadri, Phys. Rev. B 69 (2004) 075117.
[19] D.J. Singh, Phys. Rev. B 55 (1997) 309.
[20] Y. Liu, T. Fujiwara, H. Yukawa, M. Morinaga, Solid State Ionics 126 (1999) 209.
[21] Y. Koyama, Y.-S. Kim, I. Tanaka, H. Adachi, Jpn. J. Appl. Phys. 38 (1999) 2024.
[22] M.E. Arroyo y de Dompablo, C. Marianetti, A. Van der Ven, G. Ceder, Phys. Rev. B 63 (2001) 144107.
[23] L. Benco, J.-L. Barras, M. Atanasov, C.A. Daul, E. Deiss, Solid State Ionics 112 (1998) 255.